Marquette University

e-Publications@Marquette

Physics Faculty Research and Publications   Physics, Department of

4-9-2013

Responses of Mn^{2+} Speciation in *Deinococcus radiodurans* and *Escherichia coli* to **γ**-Radiation by Advanced Paramagnetic Resonance Methods

Ajay Sharma
Northwestern University

Elena K. Gaidamakova
Uniformed Services University of the Health Sciences

Vera Y. Matrosova
Uniformed Services University of the Health Sciences

Brian Bennett
Marquette University, brian.bennett@marquette.edu

Michael J. Daly
Uniformed Services University of the Health Sciences

See next page for additional authors

Follow this and additional works at: https://epublications.marquette.edu/physics_fac

Part of the Physics Commons

Authors

Ajay Sharma, Elena K. Gaidamakova, Vera Y. Matrosova, Brian Bennett, Michael J. Daly, and Brian M. Hoffman

Physics Faculty Research and Publications/College of Arts and Sciences

Responses of Mn²⁺ Speciation in *Deinococcus radiodurans* and *Escherichia coli* to γ-radiation by Advanced Paramagnetic Resonance Methods

Ajay Sharma
Department of Chemistry, Northwestern University, Evanston, IL
Elena K. Gaidamakova
Department of Pathology, School of Medicine, Uniformed Services University of the Health Sciences, Bethesda, MD
Vera Y. Matrosova
Department of Pathology, School of Medicine, Uniformed Services University of the Health Sciences, Bethesda, MD
Brian Bennett
Department of Biophysics, Medical College of Wisconsin, Milwaukee, WI
Michael J. Daly

Department of Pathology, School of Medicine, Uniformed Services University of the Health Sciences, Bethesda, MD

Brian M. Hoffman

Department of Chemistry, Northwestern University, Evanston, IL

Abstract

The remarkable ability of bacterium *Deinococcus radiodurans* to survive extreme doses of γ-rays (12,000 Gy), 20 times greater than *Escherichia coli*, is undiminished by loss of Mn-dependent superoxide dismutase (SodA). *D. radiodurans* radiation resistance is attributed to the accumulation of low-molecular-weight (LMW) "antioxidant" Mn^{2+}–metabolite complexes that protect essential enzymes from oxidative damage. However, in vivo information about such complexes within *D. radiodurans* cells is lacking, and the idea that they can supplant reactive-oxygen-species (ROS)–scavenging enzymes remains controversial. In this report, measurements by advanced paramagnetic resonance techniques [electron-spin-echo (ESE)-EPR/electron nuclear double resonance/ESE envelope modulation (ESEEM)] reveal differential details of the in vivo Mn^{2+} speciation in *D. radiodurans* and *E. coli* cells and their responses to 10 kGy γ-irradiation. The Mn^{2+} of *D. radiodurans* exists predominantly as LMW complexes with nitrogenous metabolites and orthophosphate, with negligible EPR signal from Mn^{2+} of SodA. Thus, the extreme radiation resistance of *D. radiodurans* cells cannot be attributed to SodA. Correspondingly, 10 kGy irradiation causes no change in *D. radiodurans* Mn^{2+} speciation, despite the paucity of holo-SodA. In contrast, the EPR signal of *E. coli* is dominated by signals from low-symmetry enzyme sites such as that of SodA, with a minority pool of LMW Mn^{2+} complexes that show negligible coordination by nitrogenous metabolites. Nonetheless, irradiation of *E. coli* majorly changes LMW Mn^{2+} speciation, with extensive binding of nitrogenous ligands created by irradiation. We infer that *E. coli* is highly susceptible to radiation-induced ROS because it lacks an adequate supply of LMW Mn antioxidants.

Keywords

Over the past 30 y, evidence has mounted for the widespread use of small manganous (Mn^{2+}) metabolite complexes in cellular defense against reactive oxygen species (ROS) such as superoxide ($O_2^{\bullet-}$) and hydrogen peroxide (H_2O_2), in addition to enzymatic mechanisms for antioxidant defense (**1–14**). The role of nonenzymatic defenses based on Mn is established by such findings as (*i*) ROS-scavenging enzymes are completely dispensable for extreme radiation resistance in Mn-accumulating prokaryotes (**1**, **2**, **6–8**, **11**) and (*ii*) limiting Mn^{2+} accumulation renders *Deinococcus radiodurans* cells radiation-sensitive and highly susceptible to protein oxidation (**1**, **9**). This nonenzymatic, Mn-dependent artillery for combating oxidative stress is manifested in cells that accumulate Mn^{2+} together with various inorganic and organic ligands (**2**, **11**, **13**, **14**), and has been best studied in the extremely radiation-resistant bacterium *D. radiodurans* (**8**). *D. radiodurans* is capable of surviving huge doses of γ-rays (12,000 Gy): 20 times greater than the bacterium *Escherichia coli*, and 3,000 times greater than most human cells in liquid culture (**2**). *D. radiodurans* can also endure high exposures to UV C radiation and decade-long periods of drying (**7**, **8**).

The remarkable survival of *D. radiodurans* cells to ionizing radiation and desiccation, which cause extensive DNA damage, has been rationalized under the hypothesis that protective mechanisms based on small-molecule Mn^{2+} antioxidants preserve the high efficiency of DNA repair and replication proteins during irradiation (**2**, **9**, **10**). The dominant form of Mn accumulated in *D. radiodurans* cells is Mn^{2+}, with no significant levels detected of Mn^{3+} or Mn^{4+} before or after exposure to 10 kGy (**1**, **9**), and the accumulation of high concentrations

of Mn^{2+} together with orthophosphate (Pi) and various organic metabolites is viewed as providing the components of "Mn antioxidants" that combat oxidative stress (11–13). When combined in vitro at physiological concentrations, these constituents interacted synergistically, forming heat (100 °C)-resistance ROS-scavenging complexes that were extremely radioprotective of proteins, but not DNA or RNA (13, 15). As the antioxidant enzymes in *D. radiodurans* and other Mn-accumulating radiation-resistant prokaryotes are dispensable for radiation resistance (1, 6, 11), evidently, low-molecular-weight (LMW) Mn^{2+}–metabolite complexes, which make up ~70% of the cytosolic Mn of *D. radiodurans* (13), can provide levels of in vivo protection from ROS that equal or exceed the ROS-scavenging capacities of antioxidant enzymes (11).

The nature of the antioxidant Mn^{2+} complexes within intact, viable *D. radiodurans* cells, and their response to radiation, has remained speculative, as there has been no means of determining Mn speciation in vivo; in particular, standard analytical procedures that disrupt cells alter speciation because Mn^{2+} complexes rapidly exchange their ligands (13), and the idea that such Mn^{2+} complexes can supplant ROS-scavenging enzymes remains controversial (2, 11, 16). We recently introduced (17) the use of advanced paramagnetic resonance techniques (18), electron spin-echo (ESE), electron paramagnetic resonance (EPR), electron nuclear double resonance (ENDOR), and ESE envelope modulation (ESEEM) spectroscopies, as a powerful, nondestructive way to study the in vivo coordination and speciation of Mn^{2+} in viable cells, examining the possible role of Mn^{2+}–Pi as a key in vivo antioxidant in the simple eukaryote yeast, *Saccharomyces cerevisiae* (17). In this report, comparative measurements by these techniques reveal details of the in vivo Mn^{2+} speciation (17) in *D. radiodurans* and *E. coli* cells, and of the responses of speciation when the cells are exposed to 10 kGy γ-irradiation. The results provide evidence that radiation protection in *Deinococcus* cells is indeed mainly mediated by Mn^{2+} complexed with metabolites, and give insights into the in vivo composition of the antioxidant complexes and their response to high doses of radiation. We further address a recent publication (16) that employs the spectroscopic approach we introduced, but questions the central role of the LMW Mn^{2+} complexes as radioprotectants.

Results

EPR.

The EPR absorption spectrum of a Mn^{2+} ion (S = 5/2) in high field is dominated by a feature centered at g-value of 2 (g-2) that is associated with transitions within the m_s = ±1/2 electron-spin manifold, as split into six lines by hyperfine interactions with the ^{55}Mn (I = 5/2) nucleus. This feature is flanked by signals from "satellite" transitions involving the other electron spin substates (m_s = ±3/2, ±5/2). The overall breadth of the pattern is proportional to the zero-field splitting (ZFS) parameter, D, whose magnitude in turn increases with deviations of the coordination sphere of the Mn^{2+} ion from spherical symmetry (19). **Fig. 1** shows the 35 GHz ESE EPR (2K) spectra of Mn^{2+} in frozen cell suspensions of *D. radiodurans* and *E. coli*, along with reference spectra of Mn^{2+}–Pi (17) and of the Mn^{2+} fosfomycin-resistance enzyme, (FosA) (20). We first discuss spectra of LMW Mn^{2+} complexes/standards (**Fig. 1** and Fig. S1), then spectra of Mn^{2+} enzymes (**Fig. 1** and Fig. S2), and in this context then discuss the spectra of the cells (**Fig. 1**).
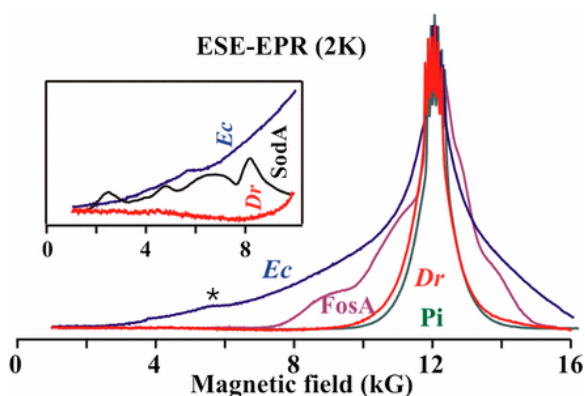
Fig. 1. ESE–EPR spectra of frozen cell suspensions of *D. radiodurans* (*Dr*) and *E. coli* (*Ec*); Pi-bound Mn^{2+}, FosA (**20**). Spectra normalized at g-2 to emphasize satellites. An asterisk indicates weak features from cellular Fe^{3+}. (*Inset*) Expanded low-field region for *D. radiodurans* (*Dr*), *E. coli* (*Ec*), and SodA (Fig. S2), normalized to equal area. Conditions: T, 2K; microwave frequency, 34.8 GHz; $t_{\pi/2}$, 60 ns; τ, 700 ns; t_{rep}, 20 ms, 50 sequences per point, 1,000 points.

The spectra of hexaaquo–Mn^{2+} and Mn^{2+}–Pi are indistinguishable (Fig. S1), with a six-line ^{55}Mn (I = 5/2) pattern centered at g-2 that "rides" on the overall g-2 feature that contains the response from the m_s = ±1/2 electron-spin manifold plus contributions from the satellite transitions; an inflection on either side of the g-2 peak leads to the broadest satellite transitions, whose intensity vanishes below ~10 kG. The aquo and phosphate complexes have a highly symmetric (octahedral) coordination geometry, and the small spread of the satellite intensity corresponds to a small ZFS ($|D| < 0.03\ cm^{-1}$). The ESE–EPR spectrum of Mn^{2+} in a solution of *N*-methylimidazole (*N*-MeIm) (Fig. S1), chosen as an intensity standard for ESEEM measurements (**21**) of *N*-coordination, exhibits a slightly broader overall envelope than *D. radiodurans* and Mn^{2+}–Pi, and a less pronounced six-line ^{55}Mn hyperfine pattern, with slightly lower ^{55}Mn hyperfine coupling than Mn^{2+}–Pi. As confirmed by ESEEM measurements below, these effects are attributable to an increase in ZFS associated with the replacement of multiple (but fewer than six overall) water oxygens of hexaaquo Mn^{2+} by nitrogens of *N*-MeIm, resulting in a suite of complexes of slightly reduced symmetry at Mn^{2+}.

Mn^{2+} in macromolecular environments can show small ZFS, for example Mn^{2+} in Con A ($|D| < 0.03\ cm^{-1}$) (**22**), but commonly shows lower symmetry and much larger ZFS (**23**, **24**), leading to more pronounced wings associated with the satellite transitions. This is illustrated by the sample enzyme spectra in **Fig. 1** and Fig. S2: as the ZFS parameter increases, the wings progressively broaden, with an accompanying broadening and splitting of the g-2 feature and loss of the six-line ^{55}Mn hyperfine pattern: FosA ($|D|$ ~0.1 cm^{-1}) (**23**) < FosA with bound substrate (FosA-S; $|D|$ ~0.2 cm^{-1}) (**23**) < Mn-dependent superoxide dismutase, SodA ($|D|$ ~0.3 cm^{-1}) (**24**). Of particular note, the resolved six-line ^{55}Mn pattern is already completely lost by $|D|$ ~0.1 cm^{-1} (FosA spectrum; Fig. S2, *Inset*). By comparison with the spectra of reference complexes and enzymes (Figs. S1 and S2), one can estimate an average of $|D|$ ~0.06–0.07 cm^{-1} for the Mn^{2+} in the *N*-MeIm solution.

The ESE–EPR spectrum of *E. coli* is distinctly different from that of hexaaquo–Mn^{2+} and phosphate-bound Mn^{2+} (**Fig. 1** and Fig. S1). The signal from the majority of Mn^{2+} in *E. coli* instead corresponds to that of the low-symmetry Mn^{2+} binding sites of enzymes such as SodA in having broad wings from auxiliary transitions whose intensity on the low-field side smoothly spreads from ~12 kG (g-2) down almost to zero (**Fig. 1**, *Inset* and Fig. S2); the smoothness of the broad wings likely reflects the superposition of signals from different enzymes with large but distinct ZFS parameters. Continuous wave (CW) and ESE–EPR spectra recorded at 9.7 GHz also are distinct from the standards (Fig. S3). On the other hand, the *E. coli* spectrum also shows a well-resolved six-line ^{55}Mn hyperfine pattern at g-2, even though this pattern is suppressed in all of the spectra of enzymes with

Mn^{2+} sites where D ≥ 0.1 cm^{-1} (Fig. S2). We interpret this superposition of sharp lines on the broad majority signal to indicate the presence of a minority population of high-symmetry Mn^{2+} ions with small ZFS, presumably the LMW complexes found in *E. coli* cells (**13**).

The ESE–EPR spectrum of late log-phase *D. radiodurans* is unlike that of *E. coli* or the enzymes, and quite similar to that of hexaaquo–Mn^{2+} and phosphate-bound Mn^{2+} (**Fig. 1** and Fig. S1), demonstrating that the *D. radiodurans* spectrum arises from Mn^{2+} with a highly symmetric coordination sphere; the majority of this signal must be associated with the ∼70% Mn^{2+} LMW complexes (**13**). Closer inspection of the *D. radiodurans* Mn^{2+} spectrum further reveals slightly broader satellite features that may be associated with LMW complexes of slightly lower symmetry or with the 30% of the Mn^{2+} associated with high-symmetry protein sites. The *D. radiodurans* spectrum is essentially identical to those obtained previously for intracellular Mn^{2+} of *S. cerevisiae* variants (Fig. S2) (**17**).

Most importantly, an expanded view of the low-field region of the ESE–EPR spectra of *D. radiodurans*, *E. coli*, and SodA (**Fig. 1**, *Inset*) shows that *D. radiodurans* exhibits no detectable intensity from the broad satellite transitions of low-symmetry Mn^{2+} bound to SodA. Whereas the majority of the Mn^{2+} of *E. coli* gives a spectrum characteristic of low-symmetry enzyme sites such as that of SodA, the absence of such a signal for *D. radiodurans* requires that no more than a few percent of total in vivo Mn^{2+} in *D. radiodurans* can be present as SodA. This is so even though the SodA polypeptide (DR1279) is constitutively expressed in *D. radiodurans* grown under the conditions used here (***Materials and Methods***) (**25**). In short, although *D. radiodurans* has accumulated high concentrations of Mn^{2+}, and must contain the SodA polypeptide, the bacterium is seen to contain negligible quantities of the functioning Mn^{2+}-bound holo-enzyme.

These observations are broadly consistent with previous studies that showed that substantially more Mn is accumulated by *D. radiodurans* (0.2–2 mM Mn) than by *E. coli* (∼0.01 mM Mn), with the majority of the "surplus" Mn^{2+} (i.e., the portion of a cell's Mn^{2+} budget not bound to proteins) likely forming LMW ROS-scavenging complexes with various metabolites (**1**, **9**, **13**).

Cellular ^{31}P and ^{1}H ENDOR Spectroscopy.

ENDOR and ESEEM spectroscopies of a paramagnetic metal ion center such as Mn^{2+} provide nuclear magnetic resonance (NMR) spectra of the nuclei that are hyperfine-coupled to the electron spin, and thus can be used to identify and characterize coordinating ligands. **Fig. 2** shows the 35 GHz Davies ENDOR spectra for the bacteria, *D. radiodurans* and *E. coli*. The frequency region from 17 to 37 MHz contains the response from the ^{31}P of phosphates bound to Mn, and that from 40 to 80 MHz from the ^{1}H of bound water (**17**, **26**). The ENDOR spectra are normalized to the ESE signal, allowing comparison of intensities for the two bacteria; numerical values for intensities of selected sharp features, denoted as ^{31}P% and ^{1}H% (**17**), are listed in Table S1. The frequencies of the ^{1}H and ^{31}P features accurately correspond to those seen previously for intracellular Mn^{2+} of the *S. cerevisiae* variants (**17**).
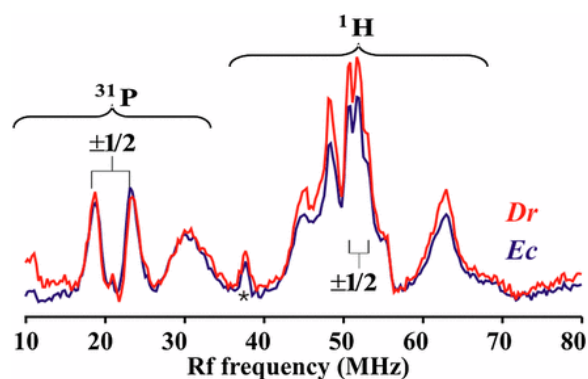
Fig. 2. Absolute Davies ENDOR spectra for *D. radiodurans* (*Dr*) and *E. coli* (*Ec*). Spectra recorded at $m_s = \pm 1/2$ low-field [55]Mn hyperfine peak, normalized to the ESE–EPR echo height. Braces show ENDOR response of ^{31}P and ^{1}H from all electron-spin manifolds ($m_s = \pm 1/2, 3/2, 5/2$). Conditions: T, 2K; microwave frequency, 34.8 GHz; $t_{\pi/2}$, 60 ns; τ, 700 ns; t_{rf}, 60 μs; t_{rep}, 20 ms, sequences/pt 300, 256 points. *Third harmonic of the [55]Mn transition.

The ^{31}P patterns for both bacteria include two sharp lines centered around the [31]P Larmor frequency separated by ~4.5 MHz. These lines are from the $m_s = \pm 1/2$ spin manifold of Mn^{2+}, and simulations show that they are associated with ^{31}P whose hyperfine coupling is almost isotropic, with isotropic coupling $A_{iso} = +5$ MHz and anisotropic component T = +0.7 MHz. In addition, the spectra contain a broad peak centered around 31 MHz with a width of 10 MHz, which is assigned to the unresolved ^{31}P ENDOR response from the outer electron spin manifolds, $m_s = \pm 3/2, 5/2$. The sharp $m_s = \pm 1/2$ peaks and observed hyperfine values exhibited by the ^{31}P ENDOR response indicate the presence of LMW complexes of Mn^{2+} bound to Pi, polyphosphates (pP) (**17**, **26**) (Fig S4), nucleotides (**27**), or nucleic acids (DNA/RNA), with Pi likely a dominant contributor (**17**) (Fig. S5). Mims pulsed ENDOR spectra (**18**) of the cells further disclose a weak ^{31}P hyperfine coupling, A ~0.3 MHz from a "second-shell" phosphate, but as such a signal is observed in solutions of Pi (Fig. S5), it does not simply distinguish between Pi and pP or nucleotide binding. Detailed decomposition of the ^{31}P spectra into component contributions (**27**) is beyond the scope of this report.

The [1]H Davies ENDOR responses for both bacteria can be assigned to protons of bound H_2O (**17**), characterized by the hyperfine values, $A_∥ = +7.6$ MHz, $A_⊥ = −2.6$ MHz, $A_{iso} = +0.8$ MHz, $A_{dip} = +3.4$ MHz (**28**); the reported hyperfine signs (**29**) have been confirmed here with a recently developed technique (pulsed ENDOR saturation and recovery, PESTRE) (**30**).

The ENDOR responses for *D. radiodurans* are dominated by LMW Mn^{2+} complexes. Stoichiometrically, in *D. radiodurans* more than twice as much Mn^{2+} is present as LMW complexes than is protein-bound (**13**), and not all Mn^{2+} proteins present bind phosphate or could show a ^{31}P signal. Indeed, the sharp ^{1}H features in the *D. radiodurans* ENDOR spectra (**Fig. 2**) are similar to those of the aquo and Pi standards (**17**), whereas the ^{1}H signals from [1]H_2O bound to a Mn^{2+} proteins commonly are broadened (**29**, **31**). The similarity of the ENDOR spectra for the two bacteria suggests a similar origin of the ENDOR signals for *E. coli*. In support of this view, we find that the ENDOR spectrum of SodA, whose ESE–EPR spectrum corresponds to that of the majority pool of low-symmetry Mn^{2+} in *E. coli*, does not have sharp ^{1}H or ^{31}P ENDOR features.

The intensities of the ^{31}P responses for *D. radiodurans* and *E. coli* are quite similar, which indicates that Mn^{2+} complexes in the two bacteria have similar average fractional populations of bound phosphates. However, the [1]H% values are unequal, *D. radiodurans* > *E. coli*, providing direct evidence for differences in the average occupancy of bound H_2O in the Mn^{2+} coordination sphere for the two organisms. A heuristic quantitation of these observations within a model for speciation is given below.

Cellular ^{14}N ESEEM Spectroscopy.

To quantitate ^{14}N ESEEM responses from Mn^{2+} in the bacteria, we chose as a standard the ^{14}N response from bound *N*-MeIm. **Fig. 3** shows the X-band three-pulse ESEEM time domain traces (*Left*) for *D. radiodurans* and *E. coli*, plus that for Mn^{2+} plus *N*-MeIm, and the ESEEM spectra (*Right*) obtained by the Fourier transform (FT) of the corresponding time domain traces. The time domain data of the Mn^{2+}/*N*-MeIm standard shows strong [14]N (I = 1) modulation. The corresponding [1]H_2O ENDOR response from the Mn^{2+}/*N*-MeIm sample is substantially suppressed, indicating that multiple *N*-Me-Im bind to each Mn^{2+} [the weakness of imidazole binding by Mn^{2+} and the fact that Mn^{2+}[imidazole]$_6$ has an extremely small ZFS (**32**) suggests that in the N-MeIm standard solution, on average each Mn^{2+} binds ~3–4 N-MeIm], displacing waters (Fig. S4).
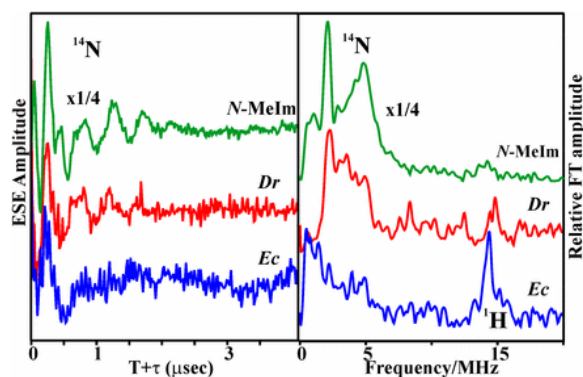
Fig. 3. Three-pulse ESEEM timewaves (*Left*) and ^{14}N spectra (***Materials and Methods***) (*Right*). Conditions: microwave frequency, 9.8 GHz; T, 10 K; magnetic field, 3,470 G; $t_{\pi/2}$, 16 ns; τ, 144 ns; interpulse time T, 200 ns incremented in 16 ns steps; t_{rep}, 0.8 ms; sequences/point, 33 (*N*-MeIm), 2,226 [*D. radiodurans* (*Dr*)], and 4,710 [*E. coli* (*Ec*)]; 256 points. ^{1}H is residual response from water protons.

The associated ESEEM spectrum (**Fig. 3**, *Right*) exhibits a strong peak at ~5 MHz, which is assigned as a double-quantum transition from ^{14}N of *N*-MeIm directly coordinated to Mn^{2+}. This frequency yields a ^{14}N hyperfine coupling of A ~3 MHz as expected from single-crystal measurements on Mn^{2+}(imidazole)$_6$ (**32**); additional weak low-frequency transitions seen in the frequency domain are primarily determined by quadrupole splittings, and a sharp feature near $2\nu_N$ ~2 MHz can be assigned to a double-quantum transition from the remote ^{14}N of coordinated *N*-MeIm. Similar hyperfine couplings also are seen for Mn^{2+} bound to nucleobases (**33**), and such a coupling thus may be taken as representative of nitrogenous ligands bound to high-spin Mn^{2+}.

The time domain trace for *D. radiodurans* shows ^{14}N modulation similar to that from the ^{14}N of *N*-MeIm (**Fig. 3**, *Left*), validating the use of this ligand as a standard. The modulation depth for *D. radiodurans* is ~20% that of the standard solution, which corresponds to an average approaching roughly one nitrogenous ligand bound to each Mn^{2+} complex of *D. radiodurans*; this interpretation is supported by the fact that the ESE–EPR spectra of *D. radiodurans* (**Fig. 1**) is not as broad as that of the *N*-MeIm standard (Fig. S1), in which Mn^{2+} binds multiple ^{14}N. The ESEEM spectra of *D. radiodurans* and Mn^{2+}/*N*-MeIm (**Fig. 3**, *Right*) both show features in the range of ~2–6 MHz, in keeping with basic similarity of the time waves from the two samples. However, the differences in peak shapes and positions from those of *N*-MeIm, along with heavier damping of the *D. radiodurans* oscillations, indicate the presence of multiple types of nitrogenous ligands.

In contrast, the time wave for *E. coli* shows extremely weak ^{14}N modulation in the 0.5–1.0 μs range (**Fig. 3**, *Left*). Importantly, this modulation decays quickly, which suggests that it arises from a variety of species with different coupling constants and with low occupancy. Oscillations evident in the time domain traces are assigned to interference effects from ^{14}N ligands with different coupling constants. Given that the low-symmetry pool dominates the EPR spectrum and Mn^{2+} binding to an enzyme invariably includes histidyl imidazole coordination, the extremely low modulation depth supports the conclusion that ENDOR/ESEEM in *E. coli* also is dominated by the LMW complexes, and that these have extremely low occupancy of nitrogenous ligands. The ESEEM spectrum for *E. coli* is weak (**Fig. 3**, *Right*), but in apparently extending to lower frequency than that from *D. radiodurans* is perhaps more similar to the *N*-MeIm spectrum than is that of *D. radiodurans*. Presumably the ^{14}N spectrum from SodA (and other enzymes) is broad, and therefore the modulation is weak and contributes little to the response.

Cellular Mn^{2+} Speciation.

The absolute ENDOR responses for Mn^{2+} complexes, ^{31}P% and ^{1}H%, for *D. radiodurans* and *E. coli* (Table S1) can be given a heuristic interpretation in terms of the fractional populations. f_i, for each of four classes of LMW species: Mn^{2+} complexes with bound (*i*) Pi, (*ii*) pP, and (*iii*) "ENDOR-silent" (ES) ligands, as well as (*iv*) the hexa-

aquo-Mn^{2+} ion (denoted Mn^{2+}-aqua, Aq) (*SI Text*) (**17**). The ESEEM results presented above now show that ES ligands of *D. radiodurans* in fact include ^{14}N-bound coordination sites as well as such truly "silent" ligands as the ^{16}O of the carboxylates of metabolites and protein side chains, etc. In this context, we will simply refer to O/N ligands as *ES*, without making distinctions. As nitrogenous ligand(s) can bind to LMW Mn^{2+} along with Pi, the simple partitioning into four classes is no longer rigorous, but it remains heuristically useful as an aid in conceptualizing the significance of differences in ^1H and ^{31}P ENDOR intensities among cell types and genetic variants (**17**), in response to growth conditions (**25**, **34**), or in response to γ radiation as in this report.

The heuristic Mn^{2+} speciation in *D. radiodurans/E. coli* is shown in **Fig. 4A** and Table S2. The $^{31}P\%$ correspond to an in vivo fraction of ~30% Mn^{2+}-bound Pi in both *D. radiodurans* and *E. coli*; neither has significant bound pP. As a result, the sum of the *ES* and hexaaquo Mn^{2+} is essentially the same for the two organisms, $(f_{ES} + f_{Aq})$ ~70%. **Fig. 4A** shows that the two populations that make up this sum show striking but inverse relationships among the two bacteria. Thus, f_{ES} ~15% for *D. radiodurans* is approximately half that of *E. coli* (30%), and f_{Aq} for *D. radiodurans* is approximately double that for *E. coli*.
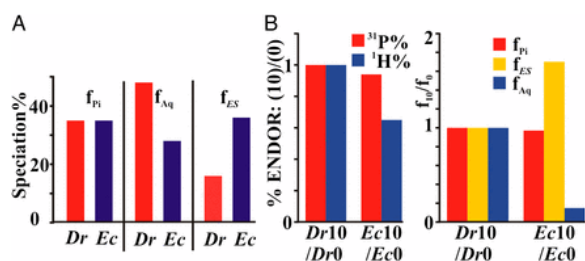

Fig. 4. (*A*) Heuristic manganese speciation: fractions of Mn^{2+} in the Pi-bound, hexaaquo, and *ES* forms in *D. radiodurans* (*Dr*) and *E. coli* (*Ec*). Fractions calculated as discussed in *SI Text*. (*B*) Effect of irradiation (10 kGy) on Mn^{2+} speciation calculated from heuristic model (*SI Text*). (*Left*) Ratio of absolute ENDOR response $[^{31}P_{10kGy}\%/^{31}P_{0kGy}\%]$, $[^1H_{10kGy}\%/^1H_{0kGy}\%]$. (*Right*) Ratio of fractions $[f_{10kGy}\%/f_{0kGy}\%]$ of Mn^{2+} bound as Pi, hexaaquo, and ES forms.

The Mn^{2+} complexes in *D. radiodurans* not only show a strong ^{14}N ESEEM response, but also a strong ^1H ENDOR response (**Fig. 2**), which is reflected in the low value of f_{ES} and high f_{Aq} (**Fig. 4A**). At minimum, these results suggest that the 70% LMW Mn^{2+} of *D. radiodurans* retains many of the waters of aqua-Mn^{2+}, in contrast, for example, to the Mn^{2+} in the high-concentration *N*-MeIm solution or to the case of pP binding (**17**). For *E. coli*, f_{ES} is higher (~1/3), although little of the Mn^{2+} binds nitrogen, so the majority of the *ES* ligands likely are carboxylates.

Changes Induced by γ-Radiation in Cellular Mn^{2+} Speciation.

γ-irradiation of *E. coli* significantly changes its ESE–EPR spectrum, broadening the auxiliary-transition "wings" (Fig. S1). Irradiation decreases the $^1H\%$ response for *E. coli* by ~1/3 while decreasing the $^{31}P\%$ only slightly (**Fig. 4B**), changes that imply a large (~50%) increase in the coordination of *ES* ligands by Mn^{2+} at the expense of the binding of water. Most dramatically, the ^{14}N modulation for Mn^{2+} in *E. coli*, which is almost absent for unirradiated *E. coli*, increases sharply upon irradiation (Fig. S6), with the radiation-induced ^{14}N ESEEM spectrum even exceeding in intensity that of *D. radiodurans* (**Fig. 5**), suggesting that the new *ES* ligands are nitrogenous species formed by radiation.
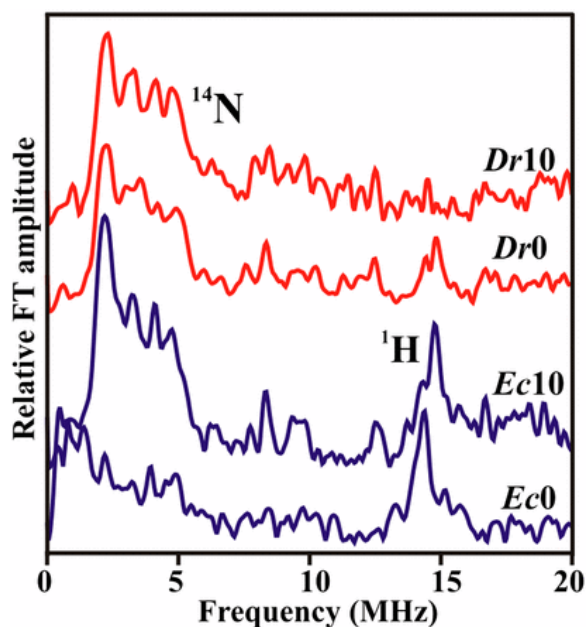
Fig. 5. Effect of irradiation on ^{14}N ESEEM spectra. Conditions same as in **Fig. 3**. *E. coli* (*Ec*) 0 and *D. radiodurans* (*Dr*) 0, no irradiation; *E. coli* 10 and *D. radiodurans* 10, 10 kGy.

In sharp contrast, none of the spectroscopic probes of Mn^{2+} showed any change induced by 10 kGy in *D. radiodurans*: (*i*) there is no significant change in the ESE–EPR spectrum (Fig. S1); (*ii*) no change in water or Pi binding, as indicated by the invariant $^{1}H\%$ or $^{31}P\%$ ENDOR responses (**Fig. 4B**); and (*iii*) none in ^{14}N binding, as indicated by the invariant ESEEM response (**Fig. 5**).

These observations together indicate that γ-radiation–induced oxidative cleavage of proteins in *E. coli* generates nitrogenous products (peptides/amino acids) that bind through ^{14}N to Mn^{2+}, replacing bound waters, whereas the proteins of *D. radiodurans* are protected.

Discussion

The accumulation of LMW Mn^{2+} complexes as a critical mechanism of surviving γ-radiation independent of SodA has been established by the findings that: (*i*) SODs and catalases are dispensable in extremely radiation-resistant Mn-accumulating prokaryotes, without a significant loss in resistance when Mn is available (**1**, **2**, **6**⇓–**8**, **11**), a finding of such key importance that we reproduce representative earlier data in Fig. S7; (*ii*) limiting Mn accumulation renders wild-type *D. radiodurans* cells highly susceptible to radiation-induced protein oxidation and killing (**1**, **9**); (*iii*) Mn-accumulating bacteria that lack SOD enzymes are able to dismutate radiation-induced $O_2^{\bullet-}$ to H_2O_2 at high efficiency (9); (*iv*) cell lysates of radiation-resistant prokaryotes contain a high abundance of heat-stable and dialyzable ROS-scavenging Mn-complexes that specifically protect proteins from γ-irradiation (**6**, **11**, **13**, **14**); and (*v*) based on size exclusion chromatography of whole-cell, protease-inhibited aqueous extracts of *D. radiodurans*, relatively little Mn is bound to proteins (**13**). As Mn^{2+} is innocuous under conditions where other biologically relevant redox-active metals (e.g., Fe) tend to promote ROS, cells can tolerate high cytoplasmic concentrations of Mn^{2+} (1–30 mM), while complexes with Pi, peptides, and nucleosides scavenge $O_2^{\bullet-}$ during irradiation, preventing the proliferation of ROS in cells (**9**, **12**, **13**) and preserving the proteome's functionality (**2**, **7**, **10**).

In this report, measurements by advanced paramagnetic resonance techniques build on these earlier findings, revealing differential details of the in vivo Mn^{2+} speciation in *D. radiodurans* and *E. coli* cells, and of the responses of speciation to 10 kGy γ-irradiation. ESE–EPR shows that the Mn^{2+} of *D. radiodurans* exists as LMW

complexes, with negligible contribution from the Mn^{2+} of holo-SodA (**Fig. 1** and Fig. S2) even though the SodA polypeptide (DR1279) is constitutively expressed in *D. radiodurans* grown under the conditions used here (**25**). Perhaps the SodA in intact *D. radiodurans* cells is being out-competed for Mn^{2+} by the accumulated LMW metabolites. Incomplete metallation of Mn-dependent enzymes has been reported for *E. coli* (**4**). Regardless, absence of ESE–EPR for SodA shows that the radiation resistance of *D. radiodurans* observed under these growth conditions (Fig. S7), and the invariance of Mn^{2+} speciation to irradiation, seen by ENDOR/ESEEM, cannot be attributed to the action of SodA. It follows that *E. coli*, whose ESE–EPR signal is dominated by signals characteristic of SodA, but is without an adequate supply of "surplus" Mn^{2+} in the form of LMW metabolite Mn^{2+} complexes, is left highly susceptible to radiation-induced ROS and protein oxidation as previously reported (**9**, **13**).

The in vivo $^{31}P/^{1}H$ ENDOR and ^{14}N ESEEM measurements show the LMW Mn^{2+} complexes in *D. radiodurans* and *E. coli* have distinctly different speciation. In both organisms, these complexes show signals associated with coordination by phosphate (and water), as expected (**3**, **11**, **13**, **17**). However, the ESEEM spectra from the complexes of *D. radiodurans* show that in intact, unirradiated cells the LMW complexes incorporate substantial amounts of nitrogenous metabolites, which give ^{14}N signals whose intensities are inferred above to correspond roughly to one nitrogen ligand per LMW Mn^{2+} complex. In contrast, the LMW complexes of unirradiated *E. coli* have extremely low occupancy of nitrogenous ligands, with noticeably different characteristics. This disparity is consistent with (*i*) the demonstrated role of nitrogenous metabolites in greatly enhancing the radioprotective properties of Mn^{2+}–Pi complexes (**13**, **15**) and (*ii*) the 10–100 times lower concentrations of such *N*-containing metabolites in *E. coli* and other radiation-sensitive bacteria (**13**).

Exposure of *D. radiodurans* to 10 kGy causes no changes in the properties or speciation of the LMW Mn^{2+} complexes, as an apparent corollary to the fact that the *D. radiodurans* cells are being protected from radiation damage mainly by these nonproteinaceous Mn antioxidants. In contrast, despite the presence of the holo-SodA in *E. coli*, the EPR spectrum of the Mn^{2+} in *E. coli* is further broadened by 10 kGy radiation, and ESEEM shows that without an adequate supply of LMW Mn^{2+} metabolite complexes in *E. coli*, the extensive protein oxidation caused by radiation-produced $O_2^{\bullet-}$ (and related ROS) yields radiation-induced nitrogenous fragment species that bind Mn^{2+}. This interpretation is consistent with the observed proteome oxidation and dysfunction in lethally irradiated *E. coli* (**10**, **13**). Following exposure to 10 kGy, *D. radiodurans* displays no significant proteome oxidation, whereas cytosolic proteins in *E. coli* are highly oxidized by just 4 kGy (**9**, **10**); protein fragmentation following 10 kGy correlates strongly with protein oxidation (**13**).

With these findings, we can briefly comment on a report that adopts the paramagnetic resonance approach we introduced (**17**) in a study of unirradiated *D. radiodurans* alone (**16**) but reaches the opposite conclusions to those presented here. The authors argue that "it is this protein (SodA) and not smaller manganese complexes…that is probably the primary defense against superoxide." In fact, their conclusion is contradicted by the studies described above (*i–v*), as extended here. In particular, we note the dispensability of SodA in radiation survival of *D. radiodurans*, *Lactobacillus plantarum*, and *Halobacterium salinarum* (as illustrated so powerfully in Fig. S7); the accumulation of an abundance of antioxidant metabolites in these extremely radiation-resistant prokaryotes (**1**, **6**, **11**); and of course, our current finding that in vivo Mn^{2+} speciation in *D. radiodurans* is invariant to 10 kGy radiation when the *D. radiodurans* cells contain negligible amounts of holo-SodA. Indeed, under growth condition where *D. radiodurans* displays increased SodA activity, the cells are more sensitive to radiation (**35**), and the estimates in the recent report of SodA concentrations in *D. radiodurans* (**16**) are far higher than supported by the available literature (**25**, **35**).

Returning to the present in vivo demonstration that nitrogenous metabolites are indeed components of antioxidant Mn complexes, to date a variety of *N*-containing metabolites accumulated in *D. radiodurans* have been identified as Mn^{2+} partners in antioxidant defense when reconstituted in vitro, including peptides (5–20

amino acids in length), uridine, uracil, adenosine, inosine, and free amino acids (**13**), and the inorganic metabolite Pi (**12**, **13**, **17**). EPR/ENDOR/ESEEM studies of Mn^{2+} bound to these candidates in vitro can help identify the functioning ligand(s) in vivo and reveal details of the cellular coordination environment of Mn^{2+}. As Mn^{2+} metabolites are becoming increasingly evident in all branches of life, and may also play an important role in microbial pathogenesis (**11**), the list of Mn-coordinating ligands that promote survival under oxidative stress is likely to expand. The advanced paramagnetic resonance techniques applied here will yield information about the structure and function of the Mn^{2+} complexes within living cells, and could further yield insights into how to better harness their radioprotective functions for practical purposes (**2**, **13**, **15**).

Materials and Methods

Sample Preparation.

Strains, growth, and irradiation conditions: *D. radiodurans* (ATCC BAA-816) and *E. coli* (K-12) (MG1655) obtained from Michael Cashel (National Institutes of Health, Bethesda, MD). For spectroscopic analysis, strains were inoculated into 200 mL tryptone/glucose/yeast extract (TGY) growth medium (**1**) in 1 L flasks, and grown in an orbital shaker at 200 rpm to OD_{600} = 1 (late log-phase). *D. radiodurans* was grown at 32 °C; *E. coli* was grown at 37 °C. For each strain, 50 mL of culture were irradiated on ice (0 °C) to 10 kGy (3 kGy/h ^{60}Co, 109–68 Irradiator, J. L. Shepherd and Associates) as described (**1**). Nonirradiated control cultures and irradiated cultures were harvested by centrifugation (*D. radiodurans*, ~10^{10} cells; *E. coli*, ~10^{10} cells). The cells were washed twice with ultrapure water, resuspended in 0.5 mL 20% Glycerol (vol/vol)/ultrapure water, then frozen at –80 °C.

EPR, ENDOR, and ESEEM Spectroscopy.

Thirty-five gigahertz ESE–EPR and Davies ENDOR spectra and the absolute ENDOR responses, ^{31}P%, ^{1}H%, were measured as described (**17**). ESEEM experiments were carried out at 10 K and 9.7 GHz using a Bruker EleXsys E580 spectrometer with EN4118×–MD4 resonator and Oxford Instruments CF935 helium flow cryostat/ITC503S temperature controller. A three-pulse sequence, π/2 - τ - π/2 - T - π/2 - τ - echo, was used with four-step phase cycling to suppress unwanted Hahn and refocused echoes. The τ is chosen to suppress the strong water protons' response. Data processing used Xepr. A third-order polynomial was subtracted from the optimally phased time-domain data. For frequency-domain spectra, a Hamming window apodization filter was applied to the background-subtracted time-domain data, the 256-point resultants were zero-filled to 512 points, and the magnitude spectra were calculated by Fourier transform. ESEEM amplitudes were normalized for the ESE amplitude.

Footnotes

- To whom correspondence may be addressed. E-mail: bmh@northwestern.edu or michael.daly@usuhs.edu.
- Author contributions: E.K.G. and V.Y.M. prepared samples; A.S. and B.B. performed research; A.S. and B.B. analyzed data; and A.S., E.K.G., V.Y.M., B.B., M.J.D., and B.M.H. wrote the paper.
- The authors declare no conflict of interest.
- This article contains supporting information online at www.pnas.org/lookup/suppl/doi:10.1073/pnas.1303376110/-/DCSupplemental.

Freely available online through the PNAS open access option.

References

1. Daly MJ, et al. (2004) Accumulation of Mn(II) in Deinococcus radiodurans facilitates gamma-radiation resistance. *Science* 306(5698):1025–1028.
2. DalyMJ (2012) Death by protein damage in irradiated cells. DNA Repair (Amst) 11(1):12–21.
3. Aguirre JD, Culotta VC (2012) Battles with iron: Manganese in oxidative stress protection. *J Biol Chem 287(17):13541–13548.*
4. Anjem A, Varghese S, Imlay JA (2009) Manganese import is a key element of the OxyR response to hydrogen peroxide in *Escherichia coli*. *Mol Microbiol* 72(4):844–858.
5. Al-Maghrebi M, Fridovich I, Benov L (2002) Manganese supplementation relieves the phenotypic deficits seen in superoxide-dismutase-null *Escherichia coli*. *Arch Biochem Biophys* 402(1):104–109.
6. Robinson CK, et al. (2011) A major role for nonenzymatic antioxidant processes in the radioresistance of Halobacterium salinarum. *J Bacteriol* 193(7):1653–1662.
7. Daly MJ (2009) A new perspective on radiation resistance based on Deinococcus radiodurans. *Nat Rev Microbiol* 7(3):237–245.
8. Slade D, Radman M (2011) Oxidative stress resistance in Deinococcus radiodurans. *Microbiol Mol Biol Re*v 75(1):133–191.
9. Daly MJ, et al. (2007) Protein oxidation implicated as the primary determinant of bacterial radioresistance. *PLoS Biol* 5(4):e92.
10. Krisko A, Radman M (2010) Protein damage and death by radiation in *Escherichia coli* and Deinococcus radiodurans. *Proc Natl Acad Sci USA* 107(32):14373–14377.
11. Culotta VC, Daly MJ (2012) Manganese complexes: Diverse metabolic routes to oxidative stress resistance in prokaryotes and yeast. *Antioxid Redox Signal*, 10.1089/ars.2012.5093.
12. Barnese K, Gralla EB, Valentine JS, Cabelli DE (2012) Biologically relevant mechanism for catalytic superoxide removal by simple manganese compounds. *Proc Natl Acad Sci USA* 109(18):6892–6897.
13. Daly MJ, et al. (2010) Small-molecule antioxidant proteome-shields in Deinococcus radiodurans. *PLoS ONE* 5(9):e12570.
14. Webb KM, DiRuggiero J (2012) Role of Mn2+ and compatible solutes in the radiation resistance of thermophilic bacteria and archaea. *Archaea* 2012:845756.
15. Gaidamakova EK, et al. (2012) Preserving immunogenicity of lethally irradiated viral and bacterial vaccine epitopes using a radio- protective Mn2+-Peptide complex from Deinococcus. *Cell Host Microbe* 12(1):117–124.
16. Tabares LC, Un S (2013) In situ determination of manganese (II) speciation in Deinococcus radiodurans by high magnetic-field EPR: Detection of high levels of Mn(II) bound to proteins. *J Biol Chem* 288(7):5050–5055.
17. McNaughton RL, et al. (2010) Probing in vivo Mn2+ speciation and oxidative stress resistance in yeast cells with ENDOR spectroscopy. *Proc Natl Acad Sci USA* 107(35):15335–15339.
18. Schweiger A, Jeschke G (2001) *Principles of Pulse Electron Paramagnetic Resonance* (Oxford Univ Press, Oxford, UK), pp 578.
19. Reed GH, Markham GD (1984) EPR of Mn(II) complexes with enzymes and other proteins. *Biological Magnetic Resonance*, eds Berliner LJ, Reuben J (Plenum, New York, London), Vol 6, pp 73–142.
20. Walsby CJ, Telser J, Rigsby RE, Armstrong RN, Hoffman BM (2005) Enzyme control of small-molecule coordination in FosA as revealed by 31P pulsed ENDOR and ESE-EPR. *J Am Chem Soc* 127(23):8310–8319.
21. McCracken J, Peisach J, Bhattacharyya L, Brewer F (1991) Electron spin echo envelope modulation studies of lectins: Evidence for a conserved Mn(2+)-binding site. *Biochemistry* 30(18):4486–4491.

22. Carmieli R, et al. (2003) Dynamics in the Mn2+ binding site in single crystals of concanavalin A revealed by high-field EPR spectroscopy. *Biochemistry* 42(25):7863–7870.
23. Smoukov SK, et al. (2002) EPR study of substrate binding to the Mn(II) active site of the bacterial antibiotic resistance enzyme FosA: A better way to examine Mn(II). *J Am Chem Soc* 124(10):2318–2326.
24. Un S, Tabares LC, Cortez N, Hiraoka BY, Yamakura F (2004) Manganese(II) zero-field interaction in cambialistic and manganese superoxide dismutases and its relationship to the structure of the metal binding site. *J Am Chem Soc* 126(9):2720–2726.
25. Lipton MS, et al. (2002) Global analysis of the Deinococcus radiodurans proteome by using accurate mass tags. *Proc Natl Acad Sci USA* 99(17):11049–11054.
26. Potapov A, Goldfarb D (2006) Quantitative characterization of the Mn2+ complexes of ADP and ATPgS by W-band ENDOR. *Appl Magn Reson* 30(3-4):461–472.
27. Kaminker I, et al. (2011) Probing conformational variations at the ATPase site of the RNA helicase DbpA by high-field electron-nuclear double resonance spectroscopy. *J Am Chem Soc* 133(39):15514–15523.
28. Tan XL, Bernardo M, Thomann H, Scholes CP (1993) Pulsed and continuous wave electron nuclear double-resonance patterns of aquo protons coordinated in frozen solution to high-spin Mn2+. *J Chem Phys* 98(7):5147–5157.
29. Manikandan P, Carmieli R, Shane T, Kalb AJ, Goldfarb D (2000) W-band ENDOR investigation of the manganese-binding site of concanavalin A: Determination of proton hyperfine couplings and their signs. *J Am Chem Soc* 122(14):3488–3494.
30. Doan PE (2011) Combining steady-state and dynamic methods for determining absolute signs of hyperfine interactions: Pulsed ENDOR saturation and recovery (PESTRE). *J Magn Reson* 208(1):76–86.
31. Tan X, Poyner R, Reed GH, Scholes CP (1993) Electron nuclear double resonance study of the Mn2+ environs in the oxalate-ATP complex of pyruvate kinase. *Biochemistry* 32(30):7799–7810.
32. Garcia-Rubio I, Angerhofer A, Schweiger A (2007) EPR and HYSCORE investigation of the electronic structure of the model complex Mn(imidazole)6: exploring Mn(II)-imidazole binding using single crystals. *J Magn Reson* 184(1):130–142.
33. Hoogstraten CG, Grant CV, Horton TE, DeRose VJ, Britt RD (2002) Structural analysis of metal ion ligation to nucleotides and nucleic acids using pulsed EPR spectroscopy. *J Am Chem Soc* 124(5):834–842.
34. Venkateswaran A, et al. (2000) Physiologic determinants of radiation resistance in Deinococcus radiodurans. *Appl Environ Microbiol* 66(6):2620–2626.
35. Chou FI, Tan ST (1990) Manganese(II) induces cell division and increases in superoxide dismutase and catalase activities in an aging deinococcal culture. *J Bacteriol* 172(4): 2029–2035.